Search for the Higgs boson
in $H \to WW^{(*)} \to \ell\ell'\nu\nu$ $(\ell,\ell' = e,\mu)$ decays with 3.0 fb^{-1} at DØ in Run II

The DØ Collaboration
URL http://www-d0.fnal.gov
(Dated: July 31, 2008)

A search for the standard model Higgs boson is presented in $H \to WW^{(*)} \to \ell\ell'\nu\nu$ $(\ell,\ell' = e,\mu,\tau)$ decays in $p\overline{p}$ collisions at a center-of-mass energy of $\sqrt{s} = 1.96$ TeV. Final states containing either two electrons, e^+e^-, an electron and a muon, $e^{\pm}\mu^{\mp}$, or two muons, $\mu^+\mu^-$, have been considered. The data sample used in this analysis has been collected between April 2002 and June 2008 by the DØ detector during Run II of the Fermilab Tevatron collider and corresponds to an integrated luminosity of 3.0 fb^{-1}. No significant excess above the background has been observed, and upper limits on the production cross section times branching ratio $\sigma \times BR(H \to WW^{(*)})$ are presented based on the combination of the three channels.

Preliminary Results for Summer Conferences 2008

I. INTRODUCTION

In the standard model (SM), the Higgs boson is crucial to the understanding of electroweak symmetry breaking and the mass generation of electroweak gauge bosons and fermions. Direct searches at the CERN e^+e^- collider (LEP) yield a lower limit for the Higgs boson mass of $m_H > 114.4$ GeV [1] at 95% confidence level (CL). Indirect measurements via fits to the electroweak precision data give an upper bound of $m_H < 190$ GeV [2] at 95% CL when taken together with the direct lower limit.

In this note a search for Higgs bosons decaying to the $WW^{(*)}$ final state in the DØ experiment at the Tevatron is presented. To achieve a good signal-to-background ratio, the leptonic decay modes $H \rightarrow WW^{(*)} \rightarrow \ell\ell'\nu\nu$ ($\ell, \ell' = e, \mu, \tau$) are considered, leading to final states containing either two electrons, e^+e^-, an electron and a muon, $e^\pm\mu^\mp$, or two muons, $\mu^+\mu^-$, and missing transverse momentum ($\not{E}_T$). The τ must decay leptonically to either a muon or electron in order to contribute to this analysis. This decay mode provides the largest sensitivity for the SM Higgs boson search at the Tevatron at a Higgs boson mass of $m_H \sim 160$ GeV [3–5]. If combined with searches exploiting the WH and ZH associated production, this decay mode also increases the sensitivity for the Higgs boson searches in the low mass region, $m_H \sim 120$ GeV.

Upper limits on the $H \rightarrow WW^{(*)} \rightarrow \ell\ell'$ cross section times branching ratio have already been presented in [6, 7]. In the present analysis, the DØ Run II data taken until June 2008 is analyzed. Upper limits on $\sigma(H) \times BR(H \rightarrow WW^{(*)})$ are presented using the combination of these three di-lepton channels.

II. DØ DETECTOR

We briefly describe the main components of the DØ Run II detector [8] important to this analysis. The central tracking system consists of a silicon microstrip tracker (SMT) and a central fiber tracker (CFT), both located within a 2 T axial magnetic field. The SMT strips have a typical pitch of 50–80 μm, and the design is optimized for tracking and vertexing over the pseudorapidity range $|\eta| < 3$, where $\eta = -\ln(\tan\frac{\theta}{2})$ with polar angle θ. The system has a six-barrel longitudinal structure, with each barrel a set of four silicon layers arranged axially around the beam pipe, interspersed with sixteen radial disks. In addition, a new layer of silicon (Layer 0) has been added just outside the beampipe in 2006. The CFT has eight thin coaxial barrels, each supporting two doublets of overlapping scintillating fibers of 0.835 mm diameter, one doublet parallel to the beam axis, the other alternating by $\pm 3°$ relative to the beam axis.

A liquid-argon/uranium calorimeter surrounds the central tracking system and consists of a central calorimeter (CC) covering to $|\eta| \approx 1.1$, and two end calorimeters (EC) extending coverage for $|\eta| < 4.2$, each housed in separate cryostats [9]. Scintillators between the CC and EC cryostats provide sampling of showers for $1.1 < |\eta| < 1.4$.

The muon system is located outside the calorimeters and consists of a layer of tracking detectors and scintillation trigger counters inside toroid magnets which provide a 1.8 T magnetic field, followed by two similar layers behind each toroid. Tracking in the muon system for $|\eta| < 1$ relies on 10 cm wide drift tubes [9], while 1 cm mini-drift tubes are used for $1 < |\eta| < 2$ [10].

III. DATA AND MC SAMPLES

The data sample used in this analysis has been collected between April 2002 and June 2008 (Run II) by the DØ detector at the Fermilab Tevatron collider at $\sqrt{s} = 1.96$ TeV, corresponding to an integrated luminosity of 3 fb^{-1}. The luminosity is calculated using the number of observed Z events in the mass region 60$< M_{\ell\ell} <$130 GeV and the NNLO $Z/\gamma^* \rightarrow ee$ ($\mu\mu$) cross section. For the $e\mu$ final state the simulations are normalized by scaling the mass distribution from the NNLO $Z/\gamma^* \rightarrow \tau\tau$ cross section to data. Data/MC electron and muon correction factors were applied to MC before normalization factors were measured. The estimated data samples were found to be consistent with the measurement of 3.0 fb^{-1} from the luminosity system within $\pm 5\%$. Some systematic uncertainties, coming from the luminosity determination or data/MC correction factors are canceled by using such a normalization procedure.

The signal and SM background processes have been simulated with PYTHIA 6.323 [11] using the CTEQ6L1 [12] parton distribution functions, followed by a detailed GEANT-based [13] simulation of the DØ detector. The signal cross sections are normalized to next-to-next-to-leading order(NNLO) calculations [14–16]. For the signal simulation gluon-gluon fusion and vector boson fusion processes are used. The $Z/\gamma^* \rightarrow \ell\ell$ cross section is calculated as $\sigma(Z/\gamma^* \rightarrow \ell\ell) = \sigma_{LO} \times K_{QCD}(Q^2)$, with the LO cross section σ_{LO} given by Pythia using LO PDF and K_{QCD} determined at NNLO with NLO CTEQ6.1M PDF according to [17]. The cross section times branching ratio of $Z/\gamma^* \rightarrow \ell\ell$ production in the invariant mass region 60 GeV $< M_{ll} < 130$ GeV is $\sigma \times BR = 241.6$ pb. The p_T distribution of $Z + jets$ events is modelled to match the Z p_T distribution measured in [18].

The $W \to l\nu$ background is calculated according to [17] with NNLO corrections and CTEQ6.1M. For inclusive W boson production with decays into a single-flavor lepton state this value is $\sigma \times BR = 2583$ pb. The calculations of [19] are used for $t\bar{t}$ production with $\sigma \times BR = 0.076$ pb with single-flavor lepton decays of both W bosons. The NLO WW, WZ and ZZ production cross section values are taken from [20] with $\sigma \times BR = 0.15$ pb for WW, $\sigma \times BR = 0.014$ pb for WZ and $\sigma \times BR = 0.002$ pb for ZZ production with decay into a single-flavor lepton state. The p_T of the WW system is modeled using the SHERPA simulation [21].

The background due to multi-jet production (called QCD fakes), when jets are misidentified as leptons, is determined from the data. A sample of like-sign di-lepton events is used in the $\mu\mu$ channel, corrected for like-sign contributions from other processes. The other channels use events with inverted lepton quality cuts, corrected to match the normalization and kinematics determined in the like-sign data.

IV. EVENT SELECTION

The $H \to WW^{(*)} \to \ell\ell'$ $(\ell, \ell' = e, \mu, \tau)$ candidates are selected by triggering on single or di-lepton events using a three level trigger system. The first trigger level uses hardware to select electron candidates based on energy deposition in the electromagnetic part of the calorimeter and muon candidates formed by hits in the muon system. Later versions of the trigger also require a high p_T central track reconstructed in the CFT by the specialized central track trigger (CTT). Digital signal processors in the second trigger level form muon track candidate segments defined by hits in the muon drift chambers and scintillators, as well as match lepton candidates to a more precise central track using additional SMT hits reconstructed by the silicon track trigger (STT). At the third level, software algorithms running on a computing farm and exploiting the full event information are used to make the final selection of events which are recorded.

In the offline analysis, electrons are identified using calorimeter and tracking information. Electromagnetic showers are identified in the calorimeter by comparing the longitudinal and transverse shower profiles to those of simulated electrons. The showers must be isolated, deposit most of their energy in the electromagnetic part of the calorimeter and pass a likelihood criterion that includes a spatial track match and, in the central detector region, an E/p requirement, where E is the energy of the calorimeter cluster and p is the momentum of the track. Electrons must be reconstructed within a detector pseudorapidity $|\eta| < 3.0$. The transverse momentum measurement of the electrons is based on calorimeter cell energy information.

Muon tracks are reconstructed from hits in the wire chambers and scintillators in the muon system and must match a track in the central tracker. To select isolated muons, the scalar sum of the transverse momentum of all tracks, other than that of the muon, in a cone of $\mathcal{R} = 0.5$ around the muon track is calculated, where $\mathcal{R} = \sqrt{(\Delta\phi)^2 + (\Delta\eta)^2}$ and ϕ is the azimuthal angle. The transverse energy deposited in the calorimeter in a hollow cone of $0.1 < \mathcal{R} < 0.4$ around the muon is also measured. In the $e\mu$ final state, both quantities are required to be < 2.5 or 4.0 GeV, depending on the Higgs mass. In the $\mu\mu$ final state, the sum of the variables divided by the muon p_T (scaled-iso) is required to be < 0.4 (0.5) for the leading (trailing) muon, and their product < 0.06. Muons are restricted to the fiducial coverage of the muon system $|\eta| < 2.0$. Muons from cosmic rays are rejected by requiring a timing criterion on the hits in the scintillator layers as well as applying restrictions on the position of the muon track with respect to the selected primary vertex.

In all final states, two leptons originating from the same primary vertex are required to be of opposite charge. Muons must have $p_T^\mu > 10$ GeV whereas electrons are required to have $p_T^e > 15$ GeV. In addition, the di-lepton invariant mass is required to exceed 15 GeV. For the di-muon final state the number of jets with $p_T > 15$ GeV is required to be $n_{\mathrm{jet}} < 2$ where jets are reconstructed in the calorimeter with a cone of radius $r_c = 0.5$. In addition both muons must be separated from a jet by $dR > 0.1$. This stage of the analysis is referred to as "pre-selection".

At this stage, the background is dominated by Z/γ^* production which is suppressed by requiring missing transverse energy $\not{E}_T > 20$ GeV. Events are further removed if the $\not{E}_T$ could have been produced by a mis-measurement of jet energies. A scaled $\not{E}_T$ variable, $\not{E}_T^{\mathrm{Scaled}}$, is used for this purpose. The jet transverse energy resolution is approximated by $\Delta E^{\mathrm{jet}} \cdot \sin\theta^{\mathrm{jet}}$ where ΔE^{jet} is proportional to $\sqrt{E^{\mathrm{jet}}}$. The opening angle $\Delta\phi\,(\mathrm{jet}, \not{E}_T)$ between this projected energy fluctuation and the missing transverse energy provides a measure of the contribution of the jet to the missing transverse energy. The scaled missing transverse energy is defined as:

$$\not{E}_T^{\mathrm{Scaled}} = \frac{\not{E}_T}{\sqrt{\sum_{\mathrm{jets}} \left(\Delta E^{\mathrm{jet}} \cdot \sin\theta^{\mathrm{jet}} \cdot \cos\Delta\phi\,(\mathrm{jet}, \not{E}_T)\right)^2}} \tag{1}$$

The minimal transverse mass M_T^{min} is the lesser transverse mass M_T built out of either of the two leptons and $\not{E}_T$,

with M_T defined as

$$M_T(l, \not{E}_T) = \sqrt{2p_T^l \not{E}_T (1 - \cos \Delta\phi(l, \not{E}_T))}. \qquad (2)$$

$M_T^{\min}$ is required to be large in order to suppress background where the $\not{E}_T$ is coming from mis-measured lepton energy. Z/γ^* boson and multi-jet events are rejected with a cut on the opening angle $\Delta\phi_{\ell\ell}$, since most of the background decays are back-to-back. This is not the case for Higgs boson decays because of the spin correlations from the scalar decay.

Some selections are final-state dependent and optimized to further suppress contributions from Z/γ^*, di-boson (WW, WZ, ZZ), $W(\to \ell\nu) + jets$, and multi-jet backgrounds. Table I shows the selection criteria used for the three different channels. Figure 1 shows the invariant ee mass and $\not{E}_T$ distributions in data, backgrounds, and signal at pre-selection for all three channels. Figure 2 shows the $\Delta\phi(\ell, \ell)$ distribution after the final selection for all three channels. As can be seen the simulation is in good agreement with data. Table II shows the number of expected and observed events after pre-selection and final selections for all three channels.

Final state	$e\mu$	ee	$\mu\mu$
Cut 0 Pre-selection	lepton ID, leptons with opposite charge and $p_T^\mu > 10$ GeV and $p_T^e > 15$ GeV invariant mass $M_{\mu\mu} > 15$ GeV $\mu\mu$: $n_{\text{jet}} < 2$ for $p_T^{\text{jet}} > 15$ GeV and $dR(\mu, \text{jet}) > 0.1$		
Cut 1 Missing Transverse Energy $\not{E}_T$ (GeV)	> 20	> 20	> 20
Cut 2 $\not{E}_T^{\text{Scaled}}$	> 7	> 6	> 5
Cut 3 $M_T^{min} (\ell, \not{E}_T)$ (GeV)	> 20	> 30	> 20
Cut 4 $\Delta\phi(\mu, \mu)$	< 2.0	< 2.0	< 2.5

TABLE I: Summary of the selection criteria for the three final states.

	$e\mu$ pre-selection	$e\mu$ final	ee pre-selection	ee final	$\mu\mu$ pre-selection	$\mu\mu$ final
$Z \to ee$	209.0 ± 3.0	0.72 ± 0.16	160463 ± 264	73.6 ± 5.1	$-$	$-$
$Z \to \mu\mu$	151.1 ± 0.6	2.14 ± 0.06	-	-	256432 ± 230	957 ± 14
$Z \to \tau\tau$	2312 ± 2	2.45 ± 0.05	835 ± 8	1.0 ± 0.3	1968 ± 11	5.5 ± 0.5
$t\bar{t}$	187.5 ± 0.2	54.2 ± 0.1	96.9 ± 0.2	28.5 ± 0.1	19.4 ± 0.1	10.1 ± 0.1
$W + jets$	163.4 ± 5.3	60.1 ± 3.2	174 ± 7	72.0 ± 4.3	149 ± 3	85.8 ± 2.1
WW	285.6 ± 0.1	108.0 ± 0.1	127.5 ± 0.4	45.7 ± 0.2	162.9 ± 0.5	91.3 ± 0.3
WZ	14.8 ± 0.1	4.9 ± 0.1	89.6 ± 0.8	7.6 ± 0.2	51.6 ± 0.5	16.2 ± 0.3
ZZ	3.47 ± 0.01	0.49 ± 0.01	73.5 ± 0.3	5.4 ± 0.1	43.0 ± 0.2	13.5 ± 0.1
Multi-jet	190 ± 168	1 ± 8	2322 ± 193	4.3 ± 8.3	945 ± 31	63.6 ± 8.0
Signal ($m_H = 160$ GeV)	9.0 ± 0.1	6.9 ± 0.1	4.40 ± 0.01	3.49 ± 0.01	4.7 ± 0.1	4.09 ± 0.06
Total Background	3516 ± 168	234 ± 9	164181 ± 327	238 ± 11	259770 ± 232	1242 ± 16
Data	3706	234	164290	236	263743	1147

TABLE II: Expected and observed number of events in each channel after pre-selection and final selections (the NN input stage). Statistical uncertainties in the expected yields are shown for all backgrounds whereas the systematic uncertainty is shown for the multi-jet background.

V. MULTIVARIATE DISCRIMINANTS

To improve the separation of signal from background, an artificial neural network (NN) is used in each of the three di-lepton channels. The NN were trained using approximately half of the background and signal events, the rest being used to test the networks' performance and to compare with data. A separate NN is trained for each Higgs boson mass tested. A weighted sum of all backgrounds was used during training.
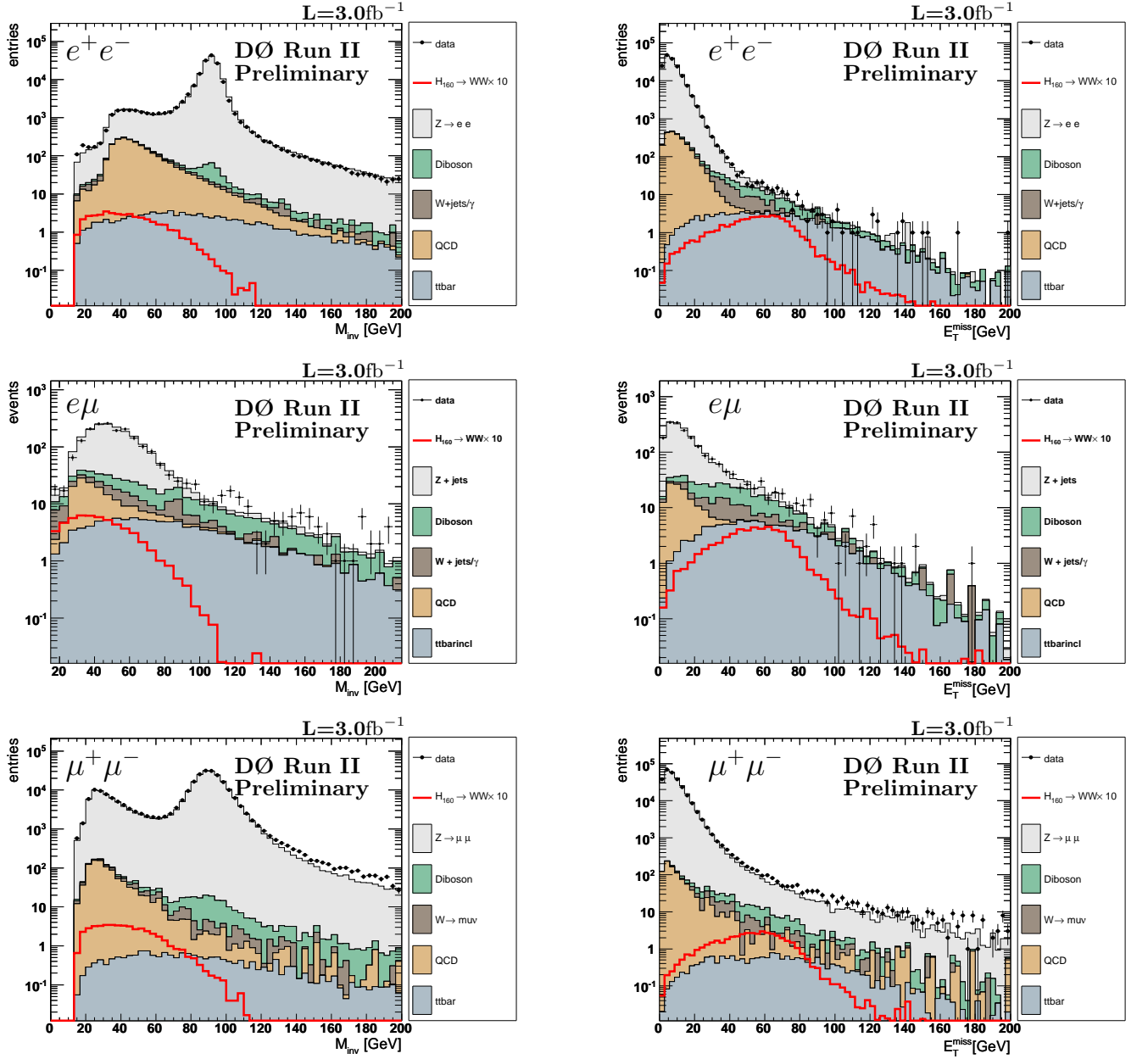
FIG. 1: Distributions of $\ell^+\ell^-$ mass (left) and $\not{E}_T$ (right) for data (points with error bars), background simulation (histograms, complemented with the QCD expectation) and signal expectation times 10 for $m_H = 160$ GeV (solid line) for the three different channels at pre-selection.

A list of input variables has been derived based on the separation power of the various distributions for each of the three channels. Those variables can be divided into three classes, lepton variables, event kinematics and angular variables. The NN input variables for the three channels are listed in Table III. The NN is applied to all events passing the final selection requirements described in Section IV. The NN output for $m_H = 160$ GeV is displayed in Figure 2 for all three channels.
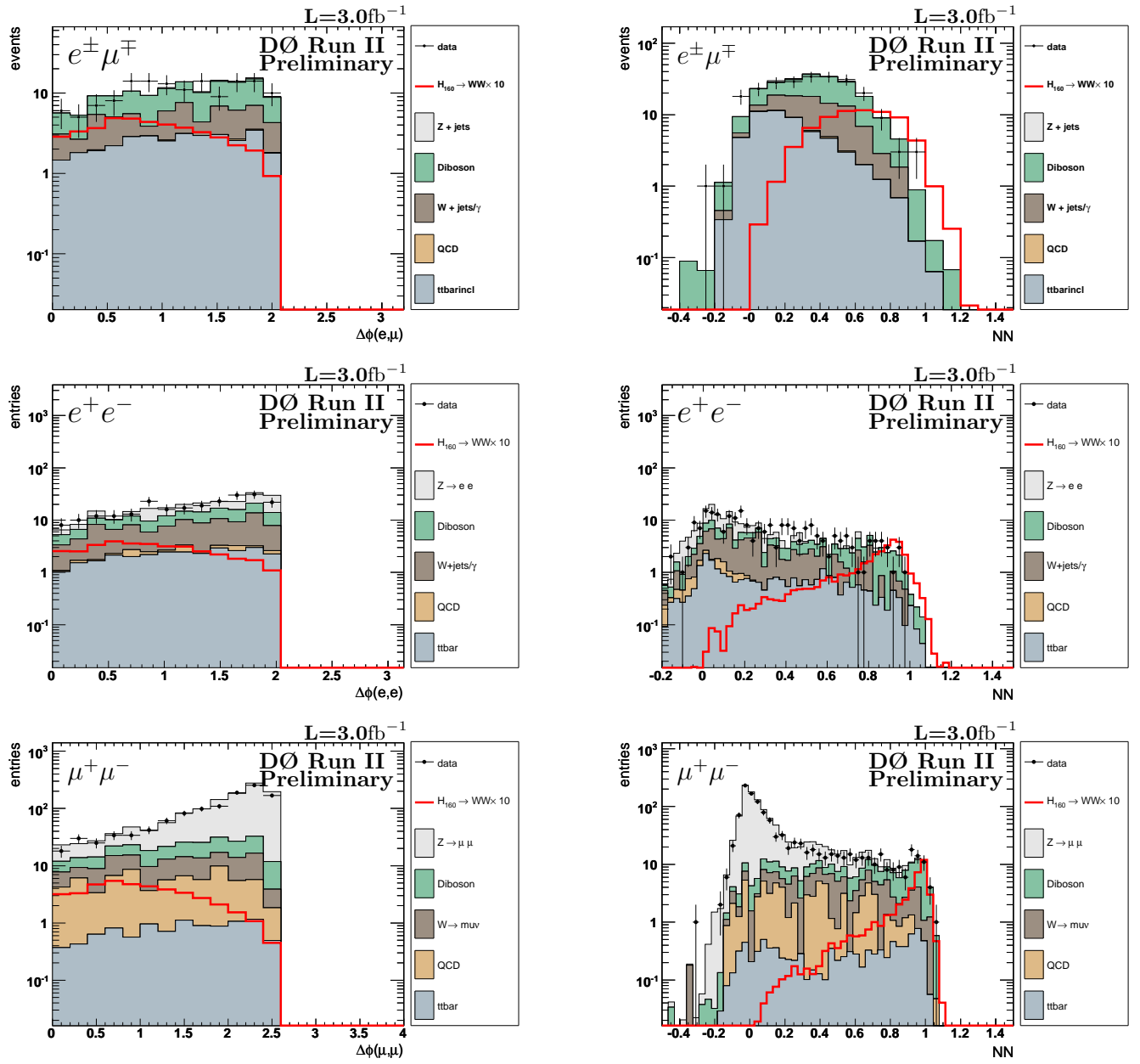
FIG. 2: Distribution of $\Delta\phi(\ell^+, \ell^-)$ (left) and the neural net output variable (right) after all selection criteria are applied for the three different channels.

NN Analysis Variables	
p_T of leading lepton	$p_T(\ell_1)$
p_T of trailing lepton	$p_T(\ell_2)$
Minimum of both lepton qualities	$\min(q_{\ell 1}, q_{\ell 2})$
Vector sum of the transverse momenta of the leptons:	$p_T(\ell_1) + p_T(\ell_2)$
Scalar sum of the transverse momenta of the jets:	$H_T = \sum_i |p_T(\text{jet}_i)|$
Invariant mass of both leptons	$M_{\text{inv}}(\ell_1, \ell_2)$
Minimal transverse mass of one lepton and $\not{E}_T$	M_T^{min}
Missing transverse energy	$\not{E}_T$
Scalar transverse energy	E_T^{scalar}
Azimuthal angle between selected leptons	$\Delta\phi(\ell_1, \ell_2)$
Solid angle between selected leptons ($e\mu$ only)	$\Theta\phi(\ell_1, \ell_2)$
ΔR between selected leptons ($e\mu$ only)	$\Delta R(\ell_1, \ell_2)$
Azimuthal angle between leading lepton and $\not{E}_T$	$\Delta\phi(\not{E}_T, \ell_1)$
Azimuthal angle between trailing lepton and $\not{E}_T$	$\Delta\phi(\not{E}_T, \ell_2)$

TABLE III: Input variables for the NN.

VI. RESULTS AND SUMMARY

The estimates for the expected number of background and signal events depend on numerous factors that each introduce a systematic uncertainty. Two different kind of systematics have been considered: flat systematics that are constant in NN and shape systematics that modify the shape of the distribution of the NN variable used for limit setting. The following flat systematics have been found: lepton reconstruction efficiencies (2.5-8%), lepton momentum calibration (2%), theoretical cross section (di-boson 7%, $t\bar{t}$ 10%, W+jet 20%), and modelling of multi-jet background (variation by factors of 2, 9, 0.1 for the ee, $e\mu$, and $\mu\mu$ final state respectively). The following systematics are implemented as shape dependent systematics: jet reconstruction efficiency (6%), jet energy scale calibration (7%), jet energy resolution (0.3%), modelling of the instantaneous luminosity (0.3%), modelling of the interaction region (1%), modelling of $p_T(WW)$, $p_T(H)$, and $p_T(Z)$ (2-33%). The systematic uncertainty on the p_T modelling has been determined by comparing the p_T distributions of PYTHIA, SHERPA, and MC@NLO. SHERPA and MC@NLO agree well with each other and generate harder p_T spectra than PYTHIA (see also [22]). The systematic uncertainty on the luminosity is mainly a combination of the PDF uncertainty, uncertainty of the NNLO Z cross section (4%) and data/MC normalization factors (2%). The total uncertainty on the background level is approximately 10% and for the signal efficiency it is 9%.

After all selection cuts, the NN output distributions in data agree within uncertainties with the expected backgrounds (see Figure 2. Thus the NN output distributions are used to set limits on the production cross section times branching ratio $\sigma \times BR(H \to WW^{(*)})$. We calculate limits for each channel and all three channels combined, using a modified frequentist method, the CLs method, with a log-likelihood ratio (LLR) test statistic [23]. To minimize the degrading effects of systematics on the search sensitivity, the individual background contributions are fitted to the data observation by maximizing a profile likelihood function for each hypothesis [24]. Figure 3 and 4 show the result of the constrained fit for the combination of all three channels before and after background subtraction. Table IV presents expected and observed upper limits at 95% CL for $\sigma \times BR(H \to WW^{(*)})$ relative to that expected in the SM for each of the three final states and for their combination for each Higgs boson mass considered.
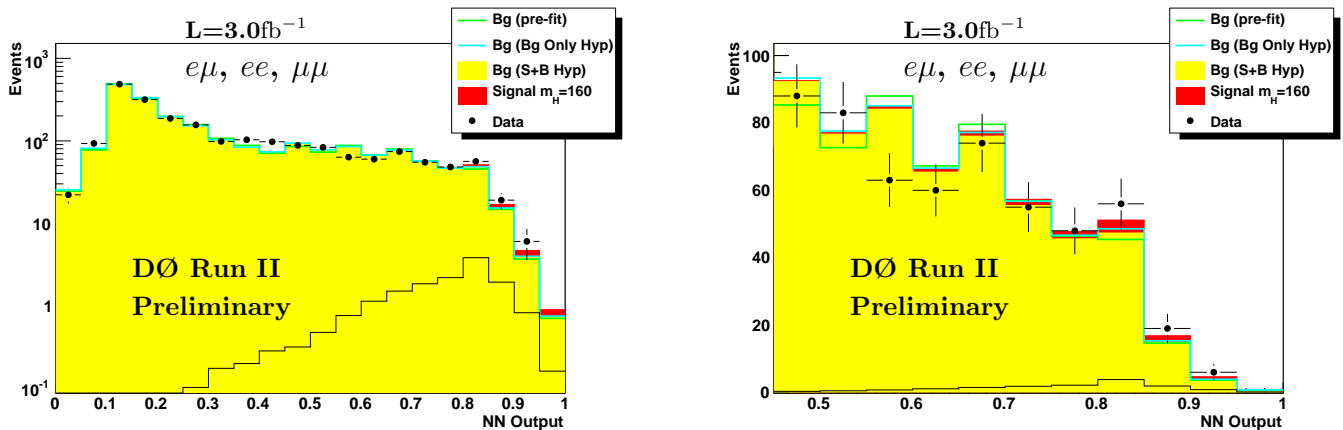

FIG. 3: Data, standard model signal expectation and background as a function of the neural net output variable. Three different background shapes are used in the analysis. The estimated background without constrained fit (pre-fit) is shown as green line. The background resulting from the constrained fit using the background-only hypothesis is shown as blue line. The background resulting from the constrained fit using the signal plus background hypothesis is shown as yellow histogram. The expected standard model signal for a Higgs boson mass of $m_H = 160$ GeV is shown as red histogram on top of the background and as black line. The neural net output is shown in logarithmic scale (left) and in linear scale for the high NN region (right).

Figure 5 shows the expected and observed limits for $\sigma \times BR(H \to WW^{(*)})$ relative to the SM for the different Higgs boson masses and the LLR distribution for the 3.0 fb^{-1} of Run II data. So far, no region of the SM Higgs mass range can be excluded, and no significant excess is observed.

[1] R. Barate *et al.*, Phys. Lett. B **565**, 61 (2003).
[2] The LEP Electroweak Working Group, *Precision Electroweak Measurements and Constraints on the Standard Model*, arXiv:0712.0929 [hep-ex] and update from March 2008 on http://lepewwg.web.cern.ch/LEPEWWG/
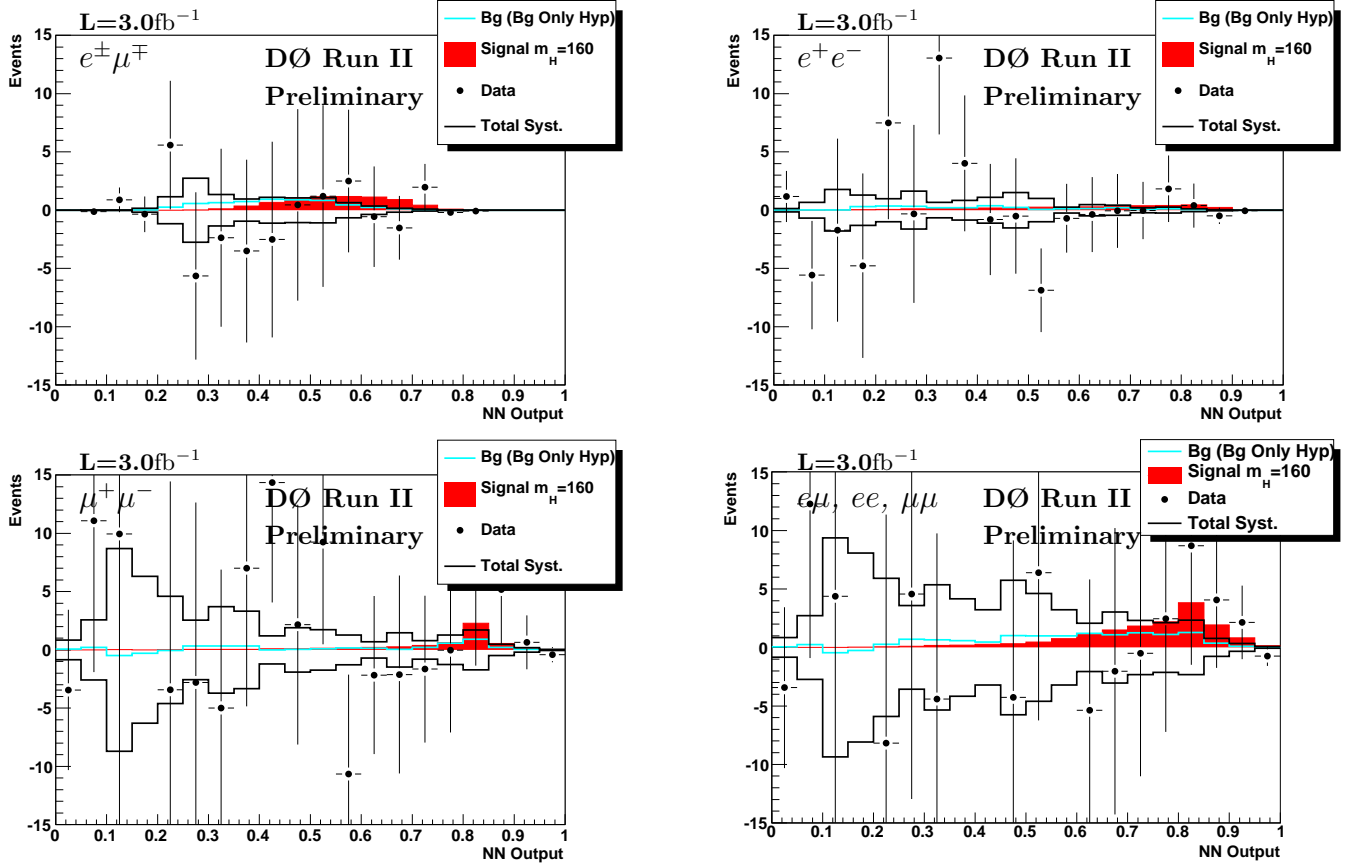
FIG. 4: Data and SM signal expectation after background subtraction as a function of the neural net output variable. The background resulting from the constrained fit using the signal plus background hypothesis is subtracted. The constrained background resulting from the background only hypothesis is shown as blue line. The standard model signal expectation is shown as red histogram. The constrained total systematic uncertainty is shown as black line.

TABLE IV: Expected and observed upper limits at 95% CL for $\sigma \times BR(H \to WW^{(*)})$ relative to the SM for e^+e^-, $e\mu$, and $\mu^+\mu^-$ final states in Run II and their combination for different Higgs boson masses (m_H).

$m_H=$	115	120	125	130	135	140	145	150	155	160	165	170	175	180	185	190	195	200
$e\mu$ (exp.)	66	37	32	18	16	13	12	7.9	6.4	4.6	4.0	4.8	5.6	6.8	9.0	11	13	15
$e\mu$ (obs.)	66	39	32	18	14	10	11	6.6	5.9	4.5	3.7	3.7	4.8	5.1	7.3	8.2	9.9	10
ee (exp.)	69	36	23	16	13	11	9.2	8.0	6.2	4.9	4.2	5.1	6.1	7.1	11	11	13	15
ee (obs.)	51	36	38	21	18	16	12	8.2	5.4	5.0	3.7	4.7	4.6	6.3	10	13	14	14
$\mu\mu$ (exp.)	47	32	23	16	13	10.0	9.6	7.8	-	6.0	5.3	6.0	7.5	8.7	11	14	16	20
$\mu\mu$ (obs.)	51	30	24	18	18	15	8.8	10	-	7.1	6.4	5.3	8.8	9.0	10	17	13	15
Run II (exp.)	24	14	11	7.0	5.8	4.9	4.2	3.3	2.8	2.1	1.9	2.3	2.8	3.3	4.6	5.5	6.7	7.7
Run II (obs.)	34	19	20	11	11	7.2	5.6	3.7	3.2	2.8	2.0	1.7	2.3	2.3	3.6	5.6	5.3	5.0

[3] T. Han, A. Turcot, R-J. Zhang, Phys. Rev. D **59**, 093001 (1999).
[4] M. Carena *et al.* [Higgs Working Group Collaboration], "Report of the Tevatron Higgs working group", hep-ph/0010338.
[5] K. Jakobs, W. Walkowiak, ATLAS Physics Note, ATL-PHYS-2000-019.
[6] DØ Collaboration, V. Abazov *et al.*, Phys. Rev. Lett. 96, 011801 (2006).
[7] DØ Collaboration, DØNote 5624, *Search for the Higgs Boson in $H \to WW^{(*)} \to \ell\ell'$ ($\ell, \ell' = e, \mu$) decays with 1.2 fb^{-1} at DØ in Run IIb*, (2007).
[8] DØ Collaboration, V. Abazov *et al.*, Nucl. Instrum. Methods Phys. Res. A. **565**, 463 (2006).
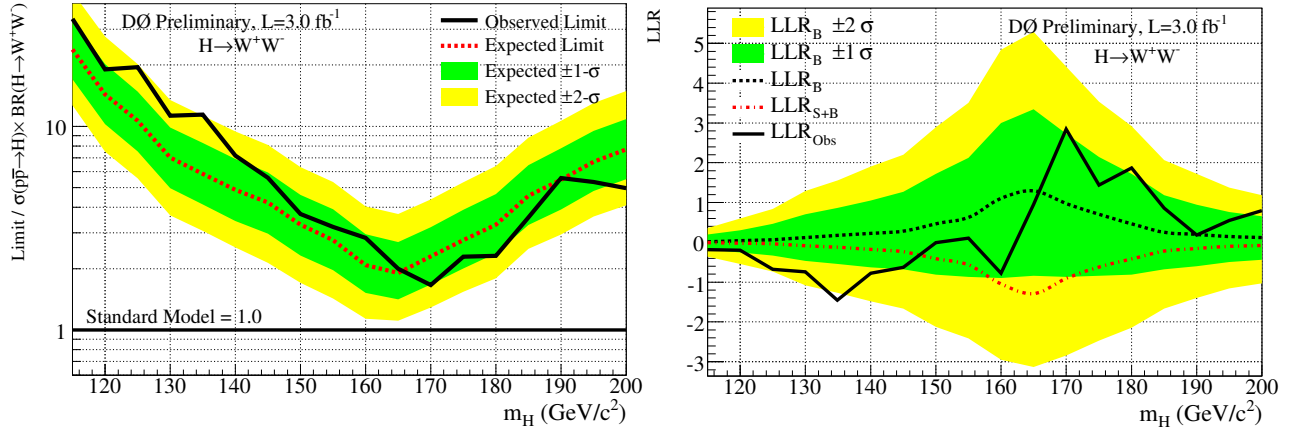[9] DØ Collaboration, S. Abachi *et al.*, Nucl. Instrum. Methods Phys. Res. A **338**, 185 (1994).

FIG. 5: Excluded cross section times branching ratio $\sigma \times BR(H \to WW^{(*)})$ at 95% CL in units of the SM cross section (left) and LLR (right) for all three channels combined, using 3.0 fb^{-1} of Run II data.

[10] V. Abramov *et al.*, Nucl. Instrum. Methods Phys. Res. A. **419**, 660 (1998).
[11] T. Sjöstrand *et al.*, Comp. Phys. Comm. **135**, 238 (2001).
[12] J. Pumplin et al., J. High Energy Phys. 07 (2002) 012.
[13] R. Brun and F. Carminati, CERN Program Library Long Writeup W5013, 1993 (unpublished).
[14] S. Catani, D. de Florian, M. Grazzini and P. Nason, JHEP **0307**, 028 (2003) [arXiv:hep-ph/0306211].
[15] K.A. Assamagan *et al.*, [Higgs Working Group Collaboration], arXiv:hep-ph/0406152
[16] U. Aglietti, R. Bonciani, G. Degrassi, A. Vicini, arXiv:hep-ph/0610033
[17] R. Hamberg, W.L. van Neerven, and T. Matsuura, Nucl. Phys. **B359**, 343 (1991) [Erratum-ibid. **B644**, 403 (2002)].
[18] DØ Collaboration, V. Abazov *et al.*, Phys. Rev. Lett. 100, 102002 (2008)
[19] N. Kidonakis and R. Vogt, Phys. Rev. D **68**, 114014 (2003).
[20] J. M. Campbell and R. K. Ellis, Phys. Rev. D **60**, 113006 (1999).
[21] T. Gleisberg, S. Höche, F. Krauss, A. Schälicke, S. Schumann and J. Winter, JHEP 0402 (2004) 056 [arXiv:hep-ph/0311263].
[22] T. Gleisberg, F. Krauss, A. Schälicke, S. Schumann and J. C. Winter, Phys. Rev. D **72**, 034028 (2005).
[23] T. Junk, Nucl. Instrum. Methods Phys. Res. A. **434**, 435 (1999). A. Read, CERN 2000-005 (30 May 2000).
[24] W. Fisher, FERMILAB-TM-2386-E.